New contributions to the drug profile of TNFα inhibitor SPD304: Affinity, selectivity and ADMET considerations

Aïda Mascret, Hadley Mouhsine, Ghada Attia, Damien Cabrera, Mohamed Benchekroun, Patrick Gizzi, Chouki Zerrouki, Najla Fourati, Jean-François Zagury, Maité Sylla-Iyarreta, et al.

▶ **To cite this version:**

Aïda Mascret, Hadley Mouhsine, Ghada Attia, Damien Cabrera, Mohamed Benchekroun, et al.. New contributions to the drug profile of TNFα inhibitor SPD304: Affinity, selectivity and ADMET considerations. European Journal of Pharmacology, 2021, 907, pp.174285. 10.1016/j.ejphar.2021.174285 . hal-03417296

HAL Id: hal-03417296
https://hal.science/hal-03417296

Submitted on 2 Aug 2023

HAL is a multi-disciplinary open access archive for the deposit and dissemination of scientific research documents, whether they are published or not. The documents may come from teaching and research institutions in France or abroad, or from public or private research centers.

L'archive ouverte pluridisciplinaire **HAL**, est destinée au dépôt et à la diffusion de documents scientifiques de niveau recherche, publiés ou non, émanant des établissements d'enseignement et de recherche français ou étrangers, des laboratoires publics ou privés.

Distributed under a Creative Commons Attribution - NonCommercial 4.0 International License

Version of Record: https://www.sciencedirect.com/science/article/pii/S0014299921004386
Manuscript_b9cbd0fa935323085a9fb7aef31649b1

New contributions to the drug profile of TNFα inhibitor SPD304: affinity, selectivity and ADMET considerations

Aïda Mascret[a,b], Hadley Mouhsine[b], Ghada Attia[c], Damien Cabrera[a], Mohamed Benchekroun[a], Patrick Gizzi[e], Chouki Zerrouki[c], Najla Fourati[c], Jean-François Zagury[a] , Maité Sylla-Iyarreta Veitia[a*], Marc Port[a*]

Affiliations

[a] *Laboratoire Génomique, Bioinformatique et Chimie Moléculaire (EA 7528), Conservatoire National des Arts et Métiers (Cnam), 2 rue Conté, 75003, HESAM Université, Paris, France.*

[b] *Peptinov, Pépinière Paris Santé Cochin,, Hôpital Cochin, 29 rue du Faubourg Saint Jacques Paris 75014*

[c] *Laboratoire SATIE, UMR CNRS 8029, Conservatoire National des Arts et Métiers (Cnam), 292 rue Saint Martin, 75003, HESAM Université, Paris, France*

[e] *PCBIS, UMS3286 CNRS - Université de Strasbourg, Boulevard Sébastien Brant, 67401 Illkirch Cedex*

*Corresponding author (E-mail address):

maite.sylla@lecnam.net (Pr. M. Sylla-Iyarreta Veitía)

marc.port@lecnam.net (Pr. M. Port)

© 2021 published by Elsevier. This manuscript is made available under the CC BY NC user license
https://creativecommons.org/licenses/by-nc/4.0/

Abstract

Tumor necrosis factor alpha (TNFα) is a relevant clinical target for the treatment of chronic inflammatory diseases. Currently, only few small molecules are known as direct inhibitors of TNFα. To date, none of these molecules has shown both an efficient activity and a low toxicity to be considered for clinical trials. The SPD304 is considered as a reference of direct inhibitors of TNFα because of its well demonstrated mechanism (He et al., 2005).

Herein, we provide new insights regarding the drug profile, selectivity and absorption, distribution, metabolism, excretion and toxicity (ADMET) considerations of SPD304 to evaluate its potential as a hit for the structure-based design of novel TNFα inhibitors. ELISA experiments confirmed the inhibition of TNFα/TNF receptor 1 binding (IC_{50} = 12 µM). Cellular-based assays highlighted the cytotoxicity of SPD304, as well as its ability to inhibit TNFα signaling pathways at non-cytotoxic concentrations. A surface acoustic wave (SAW) experiment highlighted only one binding site with a dissociation constant of 6.1 ± 4.7 nM. SPD304 inhibited the binding of the cytokines like interleukins (IL)-4 and IL-13 to their receptors and showed no direct inhibition on proteins involved in the TNFα pathway. Finally, the thermodynamic solubility and Caco-2 cells permeability of SPD304 were experimentally evaluated and ADMET *in silico* predictions are also discussed. The physicochemical, pharmacological and ADMET studies of SPD304 have shown that is not an ideal hit for a drug optimization program based on its chemical structure.

Keywords: *SPD304, Surface Acoustic Wave biosensor, Thermodynamic solubility, TNFα, ADMET*

1. Introduction

Cytokines are proteins with a molar mass of between 6-60 kDa, often glycosylated, synthesized by many cell types and acting on multiple cell targets, via specific membrane receptors. Beyond the innate and adaptive immunity, cytokines have a major role in diverse functions including immune cell differentiation, inflammation, angiogenesis, tumorigenesis, neurobiology, viral pathogenesis, atherosclerosis and cancer (Gulati et al., 2016).

Tumor necrosis factor alpha (TNFα) is a homotrimeric cytokine of the immune system which overproduction has been associated with several chronic inflammatory diseases such as rheumatoid arthritis, inflammatory bowel diseases and psoriasis (Aggarwal, 2003). These diseases are a major public health issue since they affect about 5% of the human population. The use of biologic therapies as an adjunct to disease modifying drugs for the treatment of autoimmune and rheumatologic diseases has now shown its clinical efficacy in many pathologies such as systemic inflammatory autoimmune diseases (Rosman et al., 2013; Her and Kavanaugh, 2016)

Since 2000, TNFα inhibition has become a major strategy for the alleviation of inflammatory diseases and molecules targeting the TNFα pathway have been a therapeutic intervention for the treatment of affected patients (Ratsimandresy et al., 2009). Several "biologics" have been developed for TNFα inhibition such as monoclonal antibodies, soluble TNFα receptor fusion proteins and recombinant TNFα binding proteins (Alizadeh et al., 2017; Richmond et al., 2015). These marketed biotherapies exhibit several drawbacks due to limited tissue penetration, route of administration, high production cost and consequently high prices, immunogenicity resulting in treatment cessation and limitation due to immune reactions (Rubbert-Roth and Finckh, 2009), and side effects, in particular an increased risk of opportunistic infections (Fleischmann et al., 2004).

To circumvent these obstacles, several research programs have been conducted to identify novel small-molecule inhibitors of TNFα (Davis and Colangelo, 2013). Among these

works, SPD304 has been identified as a reference small molecule to inhibit TNFα activity by disrupting the protein trimerization (He et al., 2005).

However, the presence of the 3-substituted indole moiety in the structure of SPD304 makes it metabolically unstable. This metabolic instability coupled to a low kinetic solubility (Papaneophytou et al., 2013) issue might explain why no further *in vivo* studies with SPD304 have been reported. SPD304 analogs with the aim to prepare less toxic and equally potent TNFα inhibitor have been described (Alexiou et al., 2014).

Hit identification from screening campaigns for drug discovery and optimization of primary hits in terms of activity but also of ADMET properties in order to derive lead compounds is an approach whose effectiveness has been demonstrated for the discovery of many drugs (Hoffer et al., 2018). This drug design approach has very recently made it possible to identify a small anti-TNFα molecule based on a 3-indolinone backbone that displays *in vivo* efficacy comparable to an anti-TNFα antibody in a mouse arthritis model (Dietrich et al., 2021). Consequently, in this work, we wanted to analyze and deepen the potential of SPD304 as a hit to evaluate whether SPD304 is an appropriate choice for the structure-based design of new TNFα inhibitors.

2. Materials and methods

2.1 *Materials*

Dimethyl sulfoxide (DMSO), bovine serum albumin (BSA), phosphate buffered saline (PBS) pH 7.4, PBS/tween 0.05% solution, 2,3-bis-(2-méthoxy-4-nitro-5-sulfophényle)-2H-tétrazolium-5-carboxanilide (XTT), thiazolyl blue tetrazolium bromide (MTT), sulfuric acid (H_2SO_4), hydrogen peroxide (H_2O_2), 11-mercaptoundecanoic acid (MUDA) and 6-mercapto-1-hexanol (MHOH) were purchased from Sigma-Aldrich (Saint Quentin Fallavier, France). 1-

ethyl-3-[3-dimethylaminopropyl] carbodiimidehydrochloride (EDC), *N*-hydroxysuccinimide (NHS), tetramethylbenzidine (TMB) and avidin-horseradish peroxydase (avidin-HRP) were from Thermo Fisher (Courtaboeuf, France). TNFα was from Proteros (Planneg, Germany).

Cytokines, their receptors, and corresponding biotinylated antibodies were obtained from Bio-Techne (Rennes, France) and Proteros. Dulbecco's modified eagle medium (DMEM), fetal bovine serum (FBS), penicillin/streptomycin, *L*-glutamine and PBS were obtained from Dutscher (Brumath, France). Actinomycin D was obtained from Fisher (Illkirch, France). L929 cell line has been grown in the Peptinov Laboratory for years (Paris, France). HEK-Blue™ TNFα, HEK-Blue™ IL-4/IL-13 cell lines and QUANTI-Blue™ were obtained from InvivoGen (Toulouse, France). Solvents, HPLC gold quality grade, were purchased from Carlo Erba (Val-de-Reuil, France).

SPD304 in a salt form (6,7-dimethyl-3-[[methyl[2-[methyl[[1-[3-(trifluoromethyl)phenyl]-1H-indol-3-yl]methyl]amino]ethyl]amino]methyl]-(4H-1-benzopyran-4-one dihydrochloride) (Fig. 1E) was synthetized on a 200 mg scale following experimental conditions modified compared to the synthesis initially proposed by He et al. (2005). SPD304 was obtained with 98% of HPLC purity and the general synthetic strategy is described in the supporting information of this article.

2.2 *TNFα/TNF receptor 1 binding enzyme-linked immunosorbent assay (ELISA)*

Microtiter plates were coated with 10 ng of TNF receptor 1 in 100 µl of PBS per well overnight at 4 °C. Serial dilutions of SPD304 (in 0.5% DMSO) were mixed with a fixed quantity of TNFα in PBS/BSA 1% and incubated 2 h at 37 °C. After blocking with PBS/BSA 2%, wells were washed and 100 µl of the mix were added to the wells and plates were incubated overnight at 4 °C. After washing, 20 ng of anti-TNFα biotinylated antibodies were added to the wells and plates were incubated for 2 h at 37 °C before addition of avidin-HRP.

After washing, TMB solution was added to wells and reaction was quenched with 1 M H_2SO_4 solution. Absorbance was measured at 450 nm with a spectrophotometer, providing the optical density (OD) of each well. Percentages of neutralization of TNFα by SPD304 were determined using the following formula:

$$\%\ Neutralization = 100 - \left(\frac{OD_{compound} - OD_{negative\ control}}{OD_{TNF\alpha} - OD_{negative\ control}} \times 100\right)$$

An IC_{50} could be computed from the percentages of neutralization.

2.3 TNFα/TNF receptor 1 equilibrium

Microtiter plates were coated with 10 ng of TNF receptor 1 in 100 µl of PBS per well overnight at 4 °C. After blocking with PBS/BSA 2%, fixed quantity of TNFα was added to the wells and plates were incubated for 2 h à 37 °C. After washing, serial dilutions of SPD304 (in 0.5% DMSO) were added to the wells and plates were incubated overnight at 4 °C. After washing, 20 ng of anti-TNFα biotinylated antibodies were added to the wells and plates were incubated for 2 h at 37 °C before addition of avidin-HRP. After washing, TMB solution was added to wells and reaction was quenched with 1 M H_2SO_4 solution. Absorbance was measured at 450 nm with a spectrophotometer providing the OD of each well. Percentages of TNFα neutralization by SPD304 were calculated as above.

2.4 TNFα/SPD304 affinity using surface acoustic wave (SAW) biosensor

2.4.1 SAW biosensor design

The designed SAW sensor consists of dual delay lines fabricated on 36° rot lithium tantalate piezoelectric substrate. The interdigital transducers, realized by evaporation of

(20/80) nm Cr/Au layers, were photolithographically patterned with a periodicity of $\lambda = 40$ µm which corresponds to an operating frequency of about 103 MHz. The measurement setup consists of a TNFα grafted SAW sensor, a Kalrez® flow cell, a poly methyl metacrylate (PMMA) cover including inletsand outlets connected to a Gilson® 3 peristaltic pump, and a HP8214 network analyser (Fig. 1). This latter was used to monitor phase output versus time at a fixed frequency.

[*Insert Fig. 1. here*]

2.4.2 Biosensors functionalization strategy

Several cleaning and activation steps were needed prior to TNFα grafting on the gold sensing area of the SAW sensor: 50 µl drop of a piranha solution (98% H_2SO_4 / 30% H_2O_2 2:1 v/v) were first deposited on the substrates, for 20 minutes, to favour the formation of OH groups on gold surfaces. The SAW devices were after that rinsed copiously with ultrapure water and then with ethanol, for 10 min, before being dried under ambient air.

Afterwards, an ethanol solution was injected on the SAW sensing area with a peristaltic pump at a constant rate of 190 µl/min before to the injection of a solution of 1 mM MUDA/10 mM MHOH in ethanol. A subsequent rinsing with ethanol and then with PBS permitted to remove the non-grafted molecules. Then, the obtained self-assembled monolayers (SAMs) were activated with: EDC/ NHS: 75 mM/ 15 mM prior to the grafting of 0.01 mg/ml of TNFα dissolved in PBS at pH 7.4. All measurements were made at room temperature.

2.5 *In cellulo studies*

2.5.1 Neutralization of cellular TNFα induced apoptosis in L929 cells

Eighty percent confluent L929 cells were plated in flat bottom plates at 4 x 10^5 cells per well in 100 µl of DMEM containing 10% FBS, 2 mM *L*-glutamine, 100 U/ml penicillin - 100 µg/ml streptomycin and incubated for one night at 37 °C, 5% CO_2. TNFα (150 pg/ml), actinomycin D (4 µg/ml) and serial dilutions of SPD304 (in 0.5% DMSO) were mixed in 150 µl DMEM medium 10% FBS, 2 mM *L*-glutamine, 100 U/ml penicillin - 100 µg/ml streptomycin in U-bottom plates. After 2 h incubation at 37 °C, 5% CO_2, 100 µl of the mix were added to the plated cells and incubated at 37 °C, 5% CO_2 for 24 h. Supernatants were discarded and 100 µl of MTT at 0.5 mg/ml were added to wells. After 2 h, supernatants were discarded and 200 µl of DMSO were then added. Plates were read at 570 nm with a spectrophotometer providing the OD of each well. Percentages of neutralization of TNFα by SPD304 were calculated using the following formula:

$$\%\ Neutralization = \left(\frac{OD_{compound} - OD_{TNF\alpha}}{OD_{negative\ control} - OD_{TNF\alpha}} \times 100 \right)$$

An IC_{50} could be computed from the percentages of neutralization.

2.5.2 Secreted embryonic alkaline phosphatase reporter assay.

Serial dilutions of SPD304 (in 0.5% DMSO) were mixed with 400 pg/ml of human TNFα, 400 ng/ml of human IL-4 or 400 ng/ml of human IL-13 in DMEM containing 10% of FBS, 2 mM *L*-glutamine, 100 U/ml penicillin - 100 µg/ml streptomycin in flat-bottom plates. After 2 h of incubation at 37 °C, 5% CO_2, 80% confluent HEK-Blue™ TNFα or IL-4/IL-13 cells were added to the mixes at 5 x 10^4 per well in DMEM containing 2 mM *L*-glutamine,

100 U/ml penicillin - 100 µg/ml streptomycin and incubated at 37 °C, 5% CO_2 for 24 h. 20 µl of supernatants were incubated for 3 h with 180 µl of QUANTI-Blue™ to reveal secretion of phosphatase alkaline and plates were read at 620 nm with a spectrophotometer, providing the OD. XTT was added to wells containing cells and incubated for 3 h and plates were read at 450 nm with a spectrophotometer providing the OD. Percentages of neutralization of TNFα by SPD304 were calculated using the following formula:

$$\%\ Neutralization = 100 - \left(\frac{OD_{compound} - OD_{negative\ control}}{OD_{cytokine} - OD_{negative\ control}} \times 100\right)$$

An IC_{50} could be computed from the percentages of neutralization.

2.6 Selectivity against other targets

2.6.1 Inhibition activity of SPD304 on kinases and caspases related to TNFα pathway

Kinases and caspases activities, implicated in TNFα pathway, were evaluated by CEREP/Eurofins (Celle-Lévescault, France) (CEREP/Eurofins, 2019) in presence of 1 µM of SPD304. The direct inhibition of SPD304 on the different kinases (IKKα, IKKβ, JNK1 & p38α) and caspases (3 and 8) was compared to control values. Data are expressed as percentages of inhibition of control values. For IKK proteins (IKKα and IKKβ), SPD304 was mixed with either IKKα or IKKβ. Enzymatic reaction was initiated with ULight™-IkappaBα substrate and ATP then incubated for 30 min (IKKα and IKKβ). SPD304 was also mixed with either p38α or JNK1. The enzymatic reactions were initiated with ULight™-myelin basic protein peptide substrate and ATP and incubated for 30 min (p38α) or 60 min (JNK1). For each experience, reactions were stopped and a labeled-anti-phospho-myelin basic protein antibody (for p38α and JNK1) or labelled-anti-phospho-IkappaBα (for IKKα and IKKβ) was

added for 60 min. After incubation, fluorescence intensity was measured using a microplate reader at 620 nm and 665 nm.

For caspases 3 and 8, SPD304 was mixed with either caspase 3 or 8 and enzymatic reaction was initiated with benzyloxycarbonyl-Ile-Glu-Thr-Asp-AFC then incubated for 30 min. Fluorescence intensity was measured using a microplate reader at 355 nm. The results were expressed as percentage of inhibition of control enzyme activity.

2.6.2 IL-4/IL-4 receptor subunit α and IL-13/IL-13 receptor α2 binding ELISA

Microtiter plates were coated with 10 ng of IL-4 receptor subunit α or IL-13 receptor α2 in 100 µl of PBS per well overnight at 4 °C. Serial dilutions of SPD304 (in 0.5% DMSO) were mixed with a fixed quantity of IL-4 or IL-13 in PBS/BSA 1% and incubated 2 h at 37 °C. After blocking with PBS/BSA 2%, wells were washed and 100 µl of the mix were added to the wells and plates were incubated overnight at 4 °C. After washing, 30 ng of anti-IL-4 or anti-IL-13 biotinylated antibodies were added to the wells and plates were incubated for 2 h at 37 °C before addition of avidin-HRP. After washing, TMB solution was added to wells and reaction was quenched with 1 M H_2SO_4 solution. Absorbance was measured at 450 nm with a spectrophotometer providing the OD of each well. Percentages of neutralization of IL-4 or IL-13 binding by SPD304 were calculated using the following formula:

$$\%\, Neutralization = 100 - \left(\frac{OD_{compound} - OD_{negative\ control}}{OD_{TNF\alpha} - OD_{negative\ control}} \times 100 \right)$$

An IC_{50} could be computed from percentages of neutralization.

2.7 Evaluation of ADME parameters

2.7.1 Thermodynamic solubility of SPD304

Thermodynamic solubility was determined by measuring the concentration of a saturated solution after equilibration. For this purpose, 1 mg of SPD304 was dissolved in 1 ml of phosphate buffer pH 7.4 and samples were prepared in duplicate. Samples were equilibrated in vertical agitator at 25 rpm, during 24 h at room temperature followed by 5 min centrifugation at 20 °C at 12820 rpm, in order to separate undissolved material. Supernatants were analyzed by ultra-performance liquid chromatography (injection of 8 µl). Solubility was determined against a single point standard prepared from a 10 mM DMSO stock solution diluted in acetonitrile/H_2O 1/1 (100 µM). Measurements were done using a Waters ACQUITY H-class series, equipped with a photo diode array as detector (max plot was used between 210 and 400 nm), controlled by Empower 3 software. The separation was performed on stationary phase of Kinetex C18 column (50 mm × 2.1 mm × 1.7 µm, 100 A) with a mobile phase composed of water (0,1 % formic acid) and acetonitrile, in gradient elution (0-0.25 min 95% H_2O/5% acetonitrile, 0.25-3.25 min 5% H_2O/95% acetonitrile, 3.25-4 min 5% H_2O/95% acetonitrile, 4-7 min 95% H_2O/5% acetonitrile), at 0.5 ml/min as flow rate. The samples were analysed at 210-400 nm.

2.7.2 Metabolic stability of SPD304

Metabolic stability was evaluated by the TechMed^{ill}/platform of integrative chemical biology of Strasbourg (Illkirch, France). Metabolic stability of SPD304 was assessed on mouse liver microsomes to determine if SPD304 was a substrate of cytochromes P450 in presence of NADPH as cofactor. Briefly, 1 µM of SPD304 (final concentration) was mixed with a 0.5 mg/ml solution of mouse liver microsomes in presence of 1 mM of NADPH and 3 mM of $MgCl_2$. After 1 h of incubation, reaction was stopped with acetonitrile and samples

were frozen. After thawing, metabolic stability of SPD304 was measured by analyzing the presence of the remaining compound (non-metabolized) in the samples by liquid chromatography coupled to tandem mass spectrometry (LC-MS/MS) using Shimadzu equipment, equipped with a triple quadrupole as detector (LC-MS 8030). The LC-MS analysis was performed on stationary phase of Kinetex C18 column (50 mm × 2.1 mm × 2.6 µm, 100 A) and mobile phase composed of water with 0.5 % formic acid (solvent A) and acetonitrile (solvent B), in a gradient elution system (0 min: 95 % A, 5 % B; 1.20 - 1.4 min: 5 % B, 95 % B; 1.42 - 2.8 min: 95 % A, 5 % B), at 0.5 ml/min as flow rate. Multiple reaction monitoring mode was used for quantitation and transition was 548.1 → 274.2, 287.3 for SPD304.

2.7.3 Caco-2 permeability assay

The permeability assay on Caco-2 cells was carried out by TechMed^{ill}/ the platform of integrative chemical biology of Strasbourg ~~(Illkirch, France)~~. Caco-2 cells were used as predictive *in vitro* model in order to evaluate the absorption of SPD304 by the intestine mucosa.

Caco-2 cells (ATCC HTB-37^{TM}) were plated in the upper chambers (apical) of a 24-well plate at 1.5x10^5 cells per well as lower chambers (basolateral) of the plate were filled with Hanks balanced salt solution. The chambers were separated with a permeable membrane. Cells were cultured at 37 °C, 5% CO_2 until transepithelial electric resistance reached 700 Ω. Then, SPD304 was placed in the upper chamber and incubated for 2 h at 37 °C, 5% CO_2. Apparent permeability of SPD304 was measured by analyzing the presence of the compound in the basolateral chamber by LC-MS/MS using Shimadzu equipment. Quantitation was performed as described in section 2.7.2.

2.7.4 ADMET predictions

In order to complete the druglikeness study, we sought to predict several ADMET features for SPD304 using the web platform ADMETlab (http://admet.scbdd.com/).(Dong et al., 2018; "Home-ADMElab: ADMET Prediction|ADMET Predictor|QSAR|ADMET Database," n.d.) This web platform is based on a vast database which is implemented with experimental ADMET data training sets collected from peer-reviewed publications, ChEMBL (Gaulton et al., 2017), EPA ("US EPA," n.d.) and DrugBank (Wishart et al., 2006) databases. Thus, it provides after processing, 288,967 unique entries to be used in the molecular similarity models.

2.7.5 Statistical analysis

All quantitative results are expressed as the mean ± standard deviation (SD).

3. Results

Initial results obtained in biological assessments using SPD304 from a commercial source (Sigma-Aldrich) were found to be non-reproducible. In order to guarantee the reproducibility of our biological studies, SPD304 ~~used~~ was synthesized in our laboratory with 98% purity by HPLC (see supplementary data).

3.1 TNFα/TNF receptor 1 binding study and TNFα/TNF receptor 1 equilibrium

Our experimental ELISA set-up confirmed that SPD304 was able to disrupt TNFα/TNF receptor 1 equilibrium. For that purpose, we incubated TNFα with serially diluted SPD304 before addition on TNF receptor 1. As shown in Fig. 2, incubation of SPD304 with TNFα prior addition on TNF receptor 1 inhibited TNFα/TNF receptor 1 binding with an IC_{50}

of 12 ± 4.5 µM. This value is of the same order of magnitude to the one published by He *et al.* (22 µM) (He et al., 2005), Alexiou et al and Melagraki et al (5 µM) using other ELISA assay (Alexiou et al., 2014; Melagraki et al., 2017).

However, when TNFα was pre-incubated with TNF receptor 1, SPD304 could also disrupt the association between TNFα and its receptor but with a milder activity. Indeed, when TNFα was prior incubated with its receptor, SPD304 disrupted the TNFα/TNF receptor 1 binding with a neutralization percentage of 26%, at 100 µM, compared to 90% when TNFα was firstly exposed to SPD304, corresponding to a decrease in the inhibitory activity of a 3.5 factor. The same results were obtained for other concentrations, SPD304 inhibitory activity is inferior when the TNFα is pre-incubated with TNF receptor 1: at 50 µM, 18% of neutralization versus 90%, and at 25 µM, 6% versus 76%. This is consistent with He et al. (2005) results, who observed that the IC_{50} of SPD304 was lower by a factor 2 in the presence of TNF receptor 1 and attributed these differences to the fact that TNF receptor 1 binding could stabilize TNFα trimer (Fig. 2).

[*Insert Fig. 2. here*]

3.2 TNFα/SPD304 affinity using SAW biosensor

Here we have designed a surface acoustic wave biosensor to estimate the dissociation constant of the TNFα/SPD304 complex. Gravimetry was investigated to determine TNFα/SPD304 affinity. This technique allows the follow-up of the kinetic of recognition between a given analyte and the corresponding recognition layer and to estimate the corresponding dissociation constants (K_d). The basic principle of gravimetric sensors consists in the measurement of changes of the velocities of surface acoustic waves, which travel along the piezoelectric substrate. Analytes detection by a given recognition layer, deposited on the

sensing area, reduces surface acoustic wave velocity, and induces thus a phase decrease of the output signal.

SAW biosensors' functionalization strategy was presented in paragraph 2.4.2. TNFα grafting on the sensing area was followed by PBS rinsing, to eliminate the non-adsorbed proteins, and once the signal stability was reached, increasing concentrations of SPD304 dissolved in PBS solution were injected. A typical gravimetric response after the injection of 10^{-5} M of SPD304 is represented in Fig. 3A. The corresponding time constant was of order of 176 ± 7 s.

[*Insert Fig. 3. here*]

The calibration curve, i.e. cumulative phase-shift variations versus cumulative SPD304 concentrations, is presented in Fig. 3B. This curve was obtained by averaging three experimental ones. Fig. 3B shows that the saturation value was of order of $2x10^{-5}$ M. The limit of detection of the designed SAW sensor, i.e the lowest detected concentration of SPD304, was equal to 1 nM. Several interaction models were then tested to estimate the dissociation constant value (K_d) between SPD304 and TNFα. The most appropriate one was a combined one site binding / Hill model:

$$\Delta\Phi(C) = \frac{A_1 \times C}{K_{d1} + C} + \frac{A_2 \times C^{\alpha}}{K_{d2}^{\alpha} + C^{\alpha}}$$

ΔΦ corresponds to phase variations for a given concentration C of SPD304, K_{d1} and K_{d2} are the first and second dissociation constants. K_{d1} is related to the TNFα/SPD304 affinity, while K_{d2} provides information on the spatial rearrangement of the protein after detection of the analytes and/or possible non-specific adsorption. A_1 and A_2 are empiric constants (their sum is equal to the saturation value of the sensor), and α is the Hill coefficient.

Dissociation constants were estimated at: K_{d1} = 6.1 ± 4.7 nM and K_{d2} = 4.2 ± 1.7 µM.

The effect of DMSO concentration, as co-solvent, on the kinetic of interaction between TNFα and SPD304 is presented in the Data in brief of this article.

3.3 In cellulo studies

In order to evaluate the inhibitory activity of SPD304 on the TNFα/TNF receptor 1 signaling pathway, we then used two cell-based assays. First, we tested SPD304 on the L929 cell line in which apoptosis is induced by TNFα. Consequently, cell survival is directly correlated with SPD304 inhibitory activity. The obtained results showed a high cytotoxicity of SPD304 from 100 µM to 25 µM (Fig. 4A). At 6.25 µM, the percentage of neutralization of TNFα was 52 % which was like the results obtained by Alexiou et al. (Alexiou et al., 2014) who described an IC_{50} of 5 µM for SPD304 in the L929 cells.

We also evaluated SPD304 in the HEK-Blue™ TNFα cell-based reporter gene assay where TNFα activity is linked to SEAP production regulated by a transcription factor, NFκB (Fig. 4B). Similar to L929 cells, SPD304 displayed high toxicity from 100 µM to 12.5 µM. At 6.25 µM, the percentage of neutralization of TNFα was 32%. Due to SPD304 cytotoxicity, we were not able to determine an accurate IC_{50} for SPD304 but the value of this IC_{50} should be between 12.5 and 6.25 µM.

[*Insert Fig. 4. here*]

3.4 Selectivity against other targets

We tested the selectivity of SPD304 for different proteins involved in the TNFα pathway. As shown in Fig. 5, 1 µM of SPD304 displayed no direct inhibition on IKKα, IKKβ

398 (IκB kinases), JNK1, p38α and caspases 3 and 8 as activities were below a cut-off value of
399 50%.
400 [*Insert Fig. 5. here*]
401
402 We then evaluated the selectivity of SPD304 for IL-4 and IL-13 (Fig. 6). First, we
403 evaluated the inhibitory activity of SPD304 for IL-4/IL-4 receptor subunit α and IL-13/IL-13
404 receptor α2 equilibria using an ELISA-based assay. Unexpectedly, we highlighted the non-
405 selectivity of the SPD304 for the inhibition of the interaction of TNFα/TNF receptor 1 as
406 SPD304 also inhibited the IL-4/IL-4 receptor subunit α and IL-13/IL-13 receptor α2
407 interactions with an IC_{50} of 6 µM and 79 µM respectively.
408 [*Insert Fig. 6. here*]
409
410 To confirm the IL-4/IL-4 receptor subunit α and IL-13/IL-13 receptor α2 inhibition,
411 SPD304 was then tested on a cell-based reporter gene assay, the HEK-Blue™ IL-4/IL-13
412 assay. SPD304 was toxic at high doses ranging from 100 µM to 12.5 µM (data not shown). At
413 6.25 µM (non-toxic dose), IL-4 and IL-13 were neutralized by SPD304 with a percentage of
414 62% and 77% respectively (calculated from QUANTI-Blue™ $OD_{450\ nm}$ using the formula
415 described in section 2.5.2) but neutralization was absent with lower doses (3.125 to 0.78 µM)
416 (Fig. 7). Due to its cytotoxicity, we were not able to determine an accurate IC_{50} for SPD304
417 but the value of this IC_{50} was between 6.25 and 3.125 µM for both cytokines.
418 [*Insert Fig. 7. here*]
419
420 *3.5. ADMET considerations of SPD304*
421

3.5.1 Thermodynamic solubility of SPD304

To assess the potential of SPD304 as a hit for an oral drug, we first evaluated the thermodynamic solubility of SPD304 in PBS, pH 7.4, insofar as this medium is representative of the extracellular fluid. SPD304 was characterized by a quite poor thermodynamic solubility of 23 ± 1 µg/ml (37 µM), which was one hundred times lower than the ideal solubility for an oral drug as optimal target for solubility would be between 500 and 3000 µg/ml for oral administration (Di et al., 2012; Sun, 2004) .

3.5.2 Metabolic stability and *Permeability on Caco-2 cells*

Metabolic stability of SPD304 was investigated in mouse liver microsomes in order to determine if SPD304 was a substrate of P450 with NADPH as a cofactor. SPD304 appeared to be poorly stable as more than 94% of the compound is metabolized after 1 h.

We investigated the permeability of SPD304 using an *in vitro* epithelial Caco-2 cell culture model. The apparent permeability of SPD304 was $0.3x10^{-6}$ $cm.s^{-1}$ corresponding to 0.6% of SPD304 able to cross Caco-2 cells monolayer in 16 h, which was a low permeability as Kerns and Di (2008).These elements showed that SPD304 is a FDA class IV compound (Center for Drug Evaluation and Research, FDA, 2017), namely poorly soluble, poorly permeable, and therefore not suitable for oral administration.

3.5.3 ADMET in silico prediction

Twenty-six ADMET endpoint predictions were computed and furnished several insights into SPD304 characteristics. The results are summarized in Table 1.

Overall, SPD304 fails to fully comply with the canonical rule of five (Lipinski et al., 1997) (i.e. Ro5), especially in terms of lipophilicity with relatively high LogP and $LogD_{7.4}$

(6.93 and 3.10, respectively), predicting poor oral adsorption. The calculated solubility is only of 0.8 µg/ml. In comparison, the experimental thermodynamic aqueous solubility value is 23 µg/ml. Furthermore, the data indicated a moderate percentage of human intestinal absorption of 80% (i.e. HIA) as well as a modest Caco-2 cells permeability of 14.9×10^{-6} cm.s^{-1}. This latter result compares unfavorably with the experimental Caco-2 cells permeability of 0.3×10^{-6} cm.s^{-1}. Lastly, SPD304 has a probability of 68% and 53% for bioavailabilities of 20% and 30%, respectively.

Projected distribution parameters showed that SPD304 is highly bound to the plasma proteins (% plasma protein binding (PPB) of 94.8%) and displays a theoretical volume of distribution of 0.422 l/kg, in line with an uniform distribution across the body. In terms of metabolism, SPD304 is predicted to inhibit all the cytochromes P450 isoforms, predominantly the 3A4 and the 2C19 isoforms. SPD304 serves also as a substrate for the 1A2, 3A4 and 2C19 isoforms. Furthermore, SPD304 showed a projected half-life of 2.24 h and a low clearance of 1.64 ml.min^{-1}.kg^{-1}. Finally, SPD304 is predicted to be a hERG channel blocker as well as non-mutagenic (Ames test) and presented a high probability of drug induced liver injury (DILI).

[*Insert Table1. here*]

4. Discussion

In this work, we provide new elements regarding the biological activity and physico-chemical characteristics of SPD304. Indeed, we recently started a drug discovery program (*Theranalpha*, n.d.) aiming to discover new small molecules inhibiting TNFα and the use of SPD304 as reference was essential to compare the activity of the new molecules. In this perspective, it seems important to complete the information concerning the drug profile and the drug likeness character of SPD304 in order to clarify if the chemical structure of SPD304 can be considered as a hit for a drug optimization program. ELISA experiments confirmed that SPD304 inhibited TNFα/TNF receptor 1 binding with an IC_{50} of 12 µM. Cellular-based assays results on two cell lines, L929 (apoptosis) and HEK-Blue™ TNFα (inflammation),

474 emphasized SPD304 cytotoxicity and also showed SPD304 ability to inhibit TNFα signaling
475 pathways at non-cytotoxic concentrations.
476 In a previous work (Moreau et al., 2016), we investigated a gravimetric SAW
477 biosensor to quantify the TNFα/SPD304 affinity and to estimate the further dissociation
478 constants (K_d). In this preliminary study, TNFα was deposited directly on the gold sensing
479 area of the SAW device, prior to the injection of increasing concentrations of SPD304. A two
480 sites model was used to fit the obtained calibration curves. The dissociation constant related to
481 TNFα/SPD304 affinity was of order of K_{d1} = (0.6 ± 0.3) µM. However, while trying to use
482 this test to systematically assess the affinity of a new library of TNFα inhibitors, we recently
483 highlighted a problem of reproducibility. We have attributed that to poorly controlled
484 adsorption of TNFα on the gold surface of the biosensor. Consequently, in the present work,
485 we investigated a novel surface functionalization strategy to guarantee a reproducible
486 anchoring of TNFα. Here, we chosen to functionalize the sensing area of the SAW sensors
487 with mixed self-assembled monolayers of 1/9 (v/v) ratio of MUDA and MHOH. This latter
488 was used as a spacer to minimize the non-specific binding of TNFα, whereas MUDA permits
489 to immobilize the protein on SAW gold surfaces (Park et al., 2011; Patel et al., 1997).
490 Thereafter, TNFα protein was grafted on the SAMs via a carbodiimide coupling reaction.
491 Details concerning the functionalization and activation steps and the corresponding
492 gravimetric results are presented in the Data in brief of this article.
493 A 103 MHz surface acoustic wave biosensor, functionalized with mixed self-
494 assembled monolayers (MUDA/MHOH, 1:9 v/v), was designed to quantify the affinity
495 between TNFα protein and SPD304 ligand. Adequate modelling of the gravimetric calibration
496 curve, with a combined one site binding and Hill mode, allowed to estimate two dissociation
497 constants at: K_{d1} = 6.1 ± 4.7 nM and K_{d2} = 4.2 ± 1.7 µM. The first dissociation constant K_{d1},
498 which is related to TNFα/SPD304 affinity, is inferior by about three orders of magnitude to

499 that of Papaneophytou et al, (Papaneophytou et al., 2013) and by about two orders of
500 magnitude to our previous work (Moreau et al., 2016). This is probably related to our
501 functionalization strategy, which allows a better grafting of TNFα protein to the SAW sensing
502 area due the use of mixed SAMs. K_{d2} value can be related to nonspecific adsorption between
503 the ligand and the protein. Hill coefficient α was of order of 0.2, indicating negative
504 cooperative interactions between SPD304 and the binding sites (Kurganov et al., 2001).
505 In terms of mechanism of action, co-crystallization showed that SPD304 displaced a
506 subunit from the trimer and bound to the resulting dimer in a folded conformation. SPD304
507 stabilized the dimeric form of TNFα by forming 16 hydrophobic contacts in particular with
508 Tyr59 and Tyr119 (protein data bank ID: 2AZ5) that are crucial to the trimer association
509 (Mukai et al., 2010). In this pioneering work (He et al., 2005), mass spectrometry
510 experiments confirmed this dissociation mechanism as 20% of the dimer was detected in
511 complex with one SPD304 molecule. He et al. in 2005, using a fluorescence homoquenching-
512 based assay, postulated that the mechanism was described by a predissociation-independent
513 model where SPD304 interacts with the TNFα trimer to form an intermediate complex which
514 promotes the TNFα monomer dissociation. This mechanism of action was further confirmed
515 by other mass spectrometry experiments (Cubrilovic et al., 2014). Our different results do not
516 call into question this predissociation-independent model mechanism. However, more
517 surprisingly, we showed in this work that SPD304 was not selective for TNFα or proteins
518 members of the TNF superfamily, such as RANKL, (Douni et al., 2011). Even if we showed
519 that SPD304 displayed no direct inhibition on proteins involved in the TNFα pathway (IκB
520 kinases, JNK1, p38α and caspases 3 et 8), we also demonstrated using biochemical (ELISA
521 tests) and cell-based assays (HEK-Blue™ cell line) that SPD304 inhibited two other
522 cytokines, IL-4 and IL-13, which are not part of the TNF superfamily. All these results taken
523 together clearly showed that the small molecule SPD304 was not selective for the inhibition

of the TNFα/TNF receptor 1 interaction. The biopharmaceutics classification system (Center for drug evaluation and research, FDA, 2017) allows differentiating drugs based on their solubility and permeability. The solubility classification is based on the highest dose strength in an immediate-release product. A drug is considered as highly soluble when the highest strength is soluble in 250 ml or less of aqueous media over the pH range of 1.0-7.5; otherwise, the drug substance is considered poorly soluble. On the other hand, a drug is considered highly permeable when its level of intestinal absorption is higher or equal to 90%, if not the drug substance is considered to be poorly permeable (Navnit H. Shah et al., 2008).

Previously, the kinetic solubility in 10 mM citrate-phosphate buffer (pH 6.5) of SPD304 had been evaluated in the literature at 10 µM (Papaneophytou et al., 2013). Even if the authors mentioned that this solubility value is not precise taking into account the experimental device used, it was significantly different from that which we measured. This difference could be explained by the different pH of measurement and by the methods of measurement (thermodynamic versus kinetic).

The thermodynamic solubility of 23 ± 1 µg/ml (37 µM), highlighted the need to improve the molecular structure of SPD304 to obtain a more soluble molecule, as poorly soluble compounds carry a higher risk of failure during development (Di et al., 2012). These elements showed that SPD304 is poorly soluble and therefore, very poorly suitable for oral administration. We also confirmed that SPD304 was a very rapidly metabolized molecule (poorly stable as more than 94% of the compound is metabolized after 1 h) and showed a low permeability on Caco-2 cells. The metabolic instability of SPD304 had been already identified by Sun and Yost, 2008. Indeed, the 3-substituted indole moiety of SPD304 is dehydrogenated by the P450 isoform, CYP3A4, producing reactive and toxic electrophilic iminium. SPD304 is also metabolized through hydroxylation, *N*-dealkylation, and epoxidation pathways (Sun and Yost, 2008). According to these authors, the 3-alkylindole moiety should be considered as

549 a toxicophoric as it is metabolically transformed into electrophilic unsaturated iminium
550 species that could react with protein and/or DNA nucleophilic residues and cause toxicities.
551 The evaluated physicochemical and pharmacological profile of SPD304 completed by
552 the ADMET *in silico* prediction makes it possible to conclude that this hit is of rather low
553 quality for a drug optimization program based on its chemical structure. In particular, the non-
554 selectivity of SPD304 constitutes a major drawback in terms of drug design of SPD304
555 analogs since non-selectivity (or promiscuity) is very often a source of adverse drug reactions
556 in animal models or clinical studies due to off-target pharmacological interactions.
557

558 ## Acknowledgments

559 This research has received funding from Agence nationale de la recherche:
560 Theranalpha grant (ANR-17-CE18-0024). We gratefully acknowledged ANRT (Association
561 nationale de la recherche et de la technologie) and Peptinov for the graduate fellowship
562 CIFRE awarded to Aïda Mascret (Grant N° 2016/0791).
563

564 ## CRediT authorship contribution statement

565 All authors contribute to the work presented in this paper. AM, HM, GA carried out
566 the biological and physicochemical studies and participates in the drafting of the article. DC
567 performed the synthesis of SPD304, PG was in charge of metabolic stability and permeability
568 studies and MB carried out the ADMET predictions. NF, CZ, J-FZ, MS-IV and MP are
569 responsible of the data analysis and the revision of the manuscript. All authors have given
570 approval to the final version of the manuscript.
571

572 ## Declaration of competing interest

573 There is no conflict of interest on this study
574

References

Afara, N., Omanovic, S., Asghari-Khiavi, M., 2012. Functionalization of a gold surface with fibronectin (FN) covalently bound to mixed alkanethiol self-assembled monolayers (SAMs): The influence of SAM composition on its physicochemical properties and FN surface secondary structure. Thin Solid Films 522, 381–389. https://doi.org/10.1016/j.tsf.2012.08.025

Aggarwal, B.B., 2003. Signalling pathways of the TNF superfamily: a double-edged sword. Nat Rev Immunol 3, 745–756. https://doi.org/10.1038/nri1184

Alexiou, P., Papakyriakou, A., Ntougkos, E., Papaneophytou, C.P., Liepouri, F., Mettou, A., Katsoulis, I., Maranti, A., Tsiliouka, K., Strongilos, A., Chaitidou, S., Douni, E., Kontopidis, G., Kollias, G., Couladouros, E., Eliopoulos, E., 2014. Rationally Designed Less Toxic SPD-304 Analogs and Preliminary Evaluation of Their TNF Inhibitory Effects. Archiv der Pharmazie 347, 798–805. https://doi.org/10.1002/ardp.201400198

Alizadeh, A.A., Hamzeh-Mivehroud, M., Farajzadeh, M., Dastmalchi, S., 2017. Identification of novel peptides against TNF-α using phage display technique and in silico modeling of their modes of binding. European journal of pharmaceutical sciences : official journal of the European Federation for Pharmaceutical Sciences 96, 490—498. https://doi.org/10.1016/j.ejps.2016.10.005

Bone, S., Alum, A., Markovski, J., Hristovski, K., Bar-Zeev, E., Kaufman, Y., Abbaszadegan, M., Perreault, F., 2018. Physisorption and chemisorption of T4 bacteriophages on amino functionalized silica particles. Journal of Colloid and Interface Science 532, 68–76. https://doi.org/10.1016/j.jcis.2018.07.107

Briand, E., Salmain, M., Compère, C., Pradier, C.-M., 2006. Immobilization of Protein A on SAMs for the elaboration of immunosensors. Colloids and Surfaces B: Biointerfaces 53, 215–224. https://doi.org/10.1016/j.colsurfb.2006.09.010

Cancino, J., Machado, S.A.S., 2012. Microelectrode array in mixed alkanethiol self-assembled monolayers: Electrochemical studies. Electrochimica Acta 72, 108–113. https://doi.org/10.1016/j.electacta.2012.04.009

Center for Drug Evaluation and Research, FDA, 2017. Waiver of In Vivo Bioavailability and Bioequivalence Studies for Immediate-Release Solid Oral Dosage Forms Based on a Biopharmaceutics Classification System. Guidance for Industry.

CEREP/Eurofins, 2019. Inhibition activity of SPD304 on kinases and caspases.

Chapman, R.G., Ostuni, E., Yan, L., Whitesides, G.M., 2000. Preparation of Mixed Self-Assembled Monolayers (SAMs) That Resist Adsorption of Proteins Using the Reaction of Amines with a SAM That Presents Interchain Carboxylic Anhydride Groups. Langmuir 16, 6927–6936. https://doi.org/10.1021/la9915791

Cubrilovic, D., Barylyuk, K., Hofmann, D., Walczak, M.J., Gräber, M., Berg, T., Wider, G., Zenobi, R., 2014. Direct monitoring of protein–protein inhibition using nano electrospray ionization mass spectrometry. Chem. Sci. 5, 2794–2803. https://doi.org/10.1039/C3SC53360C

Davis, J.M., Colangelo, J., 2013. Small-molecule inhibitors of the interaction between TNF and TNFR. Future Med Chem 5, 69–79. https://doi.org/10.4155/fmc.12.192

Di, L., Fish, P.V., Mano, T., 2012. Bridging solubility between drug discovery and development. Drug Discovery Today 17, 486–495. https://doi.org/10.1016/j.drudis.2011.11.007

Dietrich, J.D., Longenecker, K.L., Wilson, N.S., Goess, C., Panchal, S.C., Swann, S.L., Petros, A.M., Hobson, A.D., Ihle, D., Song, D., Richardson, P., Comess, K.M., Cox, P.B., Dombrowski, A., Sarris, K., Donnelly-Roberts, D.L., Duignan, D.B., Gomtsyan, A., Jung, P., Krueger, A.C., Mathieu, S., McClure, A., Stoll, V.S., Wetter, J., Mankovich, J.A., Hajduk, P.J., Vasudevan, A., Stoffel, R.H., Sun, C., 2021. Development of Orally Efficacious Allosteric Inhibitors of TNFα via Fragment-Based

627 Drug Design. J. Med. Chem. 64, 417–429.
628 https://doi.org/10.1021/acs.jmedchem.0c01280
629 Dong, J., Wang, N.-N., Yao, Z.-J., Zhang, L., Cheng, Y., Ouyang, D., Lu, A.-P., Cao, D.-S.,
630 2018. ADMETlab: a platform for systematic ADMET evaluation based on a
631 comprehensively collected ADMET database. Journal of Cheminformatics 10, 29.
632 https://doi.org/10.1186/s13321-018-0283-x
633 Douni, E., Rinotas, V., Makrinou, E., Zwerina, J., Penninger, J.M., Eliopoulos, E., Schett, G.,
634 Kollias, G., 2011. A RANKL G278R mutation causing osteopetrosis identifies a
635 functional amino acid essential for trimer assembly in RANKL and TNF. Human
636 Molecular Genetics 21, 784–798. https://doi.org/10.1093/hmg/ddr510
637 Edward H. Kerns, Li Di, n.d. 2008. Drug-like properties: concepts, structure design and
638 methods. From ADME to toxicity optimization, 1st ed. Elsevier.ISBN 978-0-12-
639 369520-8
640 Fleischmann, R.M., Iqbal, I., Stern, R.L., 2004. Considerations with the use of biological
641 therapy in the treatment of rheumatoid arthritis. Expert Opin Drug Saf 3, 391–403.
642 https://doi.org/10.1517/14740338.3.5.391
643 Gaulton, A., Hersey, A., Nowotka, M., Bento, A.P., Chambers, J., Mendez, D., Mutowo, P.,
644 Atkinson, F., Bellis, L.J., Cibrián-Uhalte, E., Davies, M., Dedman, N., Karlsson, A.,
645 Magariños, M.P., Overington, J.P., Papadatos, G., Smit, I., Leach, A.R., 2017. The
646 ChEMBL database in 2017. Nucleic Acids Res 45, D945–D954.
647 https://doi.org/10.1093/nar/gkw1074
648 Gulati, K., Guhathakurta, S., Joshi, J., Jain, N., Ray, A., 2016. Cytokines and their Role in
649 Health and Disease: A Brief Overview. MOJ Immunol 4, 1–9.
650 https://doi.org/10.15406/moji.2016.04.00121
651 He, M.M., Smith, A.S., Oslob, J.D., Flanagan, W.M., Braisted, A.C., Whitty, A., Cancilla,
652 M.T., Wang, J., Lugovskoy, A.A., Yoburn, J.C., Fung, A.D., Farrington, G., Eldredge,

J.K., Day, E.S., Cruz, L.A., Cachero, T.G., Miller, S.K., Friedman, J.E., Choong, I.C., Cunningham, B.C., 2005. Small-molecule inhibition of TNF-alpha. Science 310, 1022–1025. https://doi.org/10.1126/science.1116304

Her, M., Kavanaugh, A., 2016. Alterations in immune function with biologic therapies for autoimmune disease. Journal of Allergy and Clinical Immunology 137, 19–27. https://doi.org/10.1016/j.jaci.2015.10.023

Hoffer, L., Muller, C., Roche, P., Morelli, Xavier., 2018. Chemistry-Driven Hit-To-Lead Optimization Guided by Structure-Based Approaches. Mol. Inf. 37, n/a. https://doi.org/10.1002/minf.201800059

Home-ADMElab: ADMET Prediction|ADMET Predictor|QSAR|ADMET Database [WWW Document], n.d. URL http://admet.scbdd.com/ (accessed 7.10.20).

Hsiao, S.-H., Wu, J.-X., Chen, H.-I., 2020. High-selectivity NOx sensors based on an Au/InGaP Schottky diode functionalized with self-assembled monolayer of alkanedithiols. Sensors and Actuators B: Chemical 305, 127269. https://doi.org/10.1016/j.snb.2019.127269

Jalal Uddin, M., Khalid Hossain, M., Hossain, M.I., Qarony, W., Tayyaba, S., Mia, M.N.H., Pervez, M.F., Hossen, S., 2017. Modeling of self-assembled monolayers (SAMs) of Octadecanethiol and Hexadecanethiol on gold (Au) and silver (Ag). Results in Physics 7, 2289–2295. https://doi.org/10.1016/j.rinp.2017.06.055

Kidakova, A., Boroznjak, R., Reut, J., Öpik, A., Saarma, M., Syritski, V., 2020. Molecularly imprinted polymer-based SAW sensor for label-free detection of cerebral dopamine neurotrophic factor protein. Sensors and Actuators B: Chemical 308, 127708. https://doi.org/10.1016/j.snb.2020.127708

Kurganov, B.I., Lobanov, A.V., Borisov, I.A., Reshetilov, A.N., 2001. Criterion for Hill equation validity for description of biosensor calibration curves. Analytica Chimica Acta 427, 11–19. https://doi.org/10.1016/S0003-2670(00)01167-3

679 Li, X., Zhang, B., Tian, L., Li, W., Zhang, H., Zhang, Q., 2015. Improvement of recognition
680 specificity of surface protein-imprinted magnetic microspheres by reducing
681 nonspecific adsorption of competitors using 2-methacryloyloxyethyl
682 phosphorylcholine. Sensors and Actuators B: Chemical 208, 559–568.
683 https://doi.org/10.1016/j.snb.2014.11.045
684 Lipinski, C.A., Lombardo, F., Dominy, B.W., Feeney, P.J., 1997. Experimental and
685 computational approaches to estimate solubility and permeability in drug discovery
686 and development settings. Advanced Drug Delivery Reviews, In Vitro Models for
687 Selection of Development Candidates 23, 3–25. https://doi.org/10.1016/S0169-
688 409X(96)00423-1
689 Magallanes, C., Aguirre, B.M., González, G.A., Méndez De Leo, L.P., 2020. Interaction of
690 aqueous Cu(II) with carboxylic acid and alcohol terminated self assembled
691 monolayers: Surface and interfacial characterization. Surface Science 692, 121529.
692 https://doi.org/10.1016/j.susc.2019.121529
693 Mazouz, Z., Mokni, M., Fourati, N., Zerrouki, C., Barbault, F., Seydou, M., Kalfat, R.,
694 Yaakoubi, N., Omezzine, A., Bouslema, A., Othmane, A., 2020. Computational
695 approach and electrochemical measurements for protein detection with MIP-based
696 sensor. Biosensors and Bioelectronics 151, 111978.
697 https://doi.org/10.1016/j.bios.2019.111978
698 Melagraki, G., Ntougkos, E., Rinotas, V., Papaneophytou, C., Leonis, G., Mavromoustakos,
699 T., Kontopidis, G., Douni, E., Afantitis, A., Kollias, G., 2017. Cheminformatics-aided
700 discovery of small-molecule Protein-Protein Interaction (PPI) dual inhibitors of tumor
701 Necrosis Factor (TNF) and Receptor Activator of NF-κB Ligand (RANKL). PLoS
702 Comput Biol 13, e1005372. https://doi.org/10.1371/journal.pcbi.1005372
703 Moreau, G., Fourati, N.N., Zerrouki, C., Mouhsine, H., Montes, M., Port, M., Veitía, M.S.-I.,
704 Zagury, J.F., Yaakoubi, N., 2016. Surface Acoustic Wave Biosensors for the

Quantification of TNF-α/SPD-304 Interaction. Procedia Engineering 168, 432–435. https://doi.org/10.1016/j.proeng.2016.11.537

Mukai, Y., Nakamura, T., Yoshikawa, M., Yoshioka, Y., Tsunoda, S., Nakagawa, S., Yamagata, Y., Tsutsumi, Y., 2010. Solution of the Structure of the TNF-TNFR2 Complex. Sci. Signal. 3, ra83. https://doi.org/10.1126/scisignal.2000954

Navnit H. Shah, Wanatanee Phuapradit, Yu-E Zahng, Harpreet Sandhu, Lin Zhang, Wassen Malick, 2008. Approaches for improving bioavalilability of poorly soluble drugs, in: Pharmaceutical Dosage Forms-Tablets. 3rd edition, ISBN 978042919115

Papaneophytou, C.P., Mettou, A.K., Rinotas, V., Douni, E., Kontopidis, G.A., 2013. Solvent Selection for Insoluble Ligands, a Challenge for Biological Assay Development: A TNF-α/SPD304 Study. ACS Med. Chem. Lett. 4, 137–141. https://doi.org/10.1021/ml300380h

Park, B.-W., Kim, D.-S., Yoon, D.-Y., 2011. Surface modification of gold electrode with gold nanoparticles and mixed self-assembled monolayers for enzyme biosensors. Korean Journal of Chemical Engineering 28, 64–70. https://doi.org/10.1007/s11814-010-0349-6

Patel, N., Davies, M.C., Hartshorne, M., Heaton, R.J., Roberts, C.J., Tendler, S.J.B., Williams, P.M., 1997. Immobilization of Protein Molecules onto Homogeneous and Mixed Carboxylate-Terminated Self-Assembled Monolayers. Langmuir 13, 6485–6490. https://doi.org/10.1021/la970933h

Ramon Colorado, T. R. Lee, 2001. Thiol-based Self-assembled Monolayers: Formation and Organization, in: Encyclopedia of Materials: Science and Technology. pp. 9332–9344.

Ramos-Castillo, C.M., Sánchez-Ochoa, F., González-Sánchez, J., Tapia, A., Canto, G., 2019. Hydrogen physisorption on palygorskite dehydrated channels: A van der Waals density functional study. International Journal of Hydrogen Energy 44, 21936–21947. https://doi.org/10.1016/j.ijhydene.2019.06.114

731 Ratner, B.D., Hoffman, A.S., 2013. Chapter I.2.12 - Physicochemical Surface Modification of
732 Materials Used in Medicine, in: Ratner, B.D., Hoffman, A.S., Schoen, F.J., Lemons,
733 J.E. (Eds.), Biomaterials Science (Third Edition). Academic Press, pp. 259–276.
734 https://doi.org/10.1016/B978-0-08-087780-8.00027-9
735 Ratsimandresey, R.A., Rappaport, J., Zagury, J.-F., 2009. Anti-cytokine therapeutics: history
736 and update. Curr Pharm Des 15, 1998–2025.
737 https://doi.org/10.2174/138161209788453130
738 Rosman, Z., Shoenfeld, Y., Zandman-Goddard, G., 2013. Biologic therapy for autoimmune
739 diseases: an update. BMC Medicine 11, 88. https://doi.org/10.1186/1741-7015-11-88
740 Rubbert-Roth, A., Finckh, A., 2009. Treatment options in patients with rheumatoid arthritis
741 failing initial TNF inhibitor therapy: a critical review. Arthritis Res Ther 11 Suppl 1,
742 S1–S1. https://doi.org/10.1186/ar2666
743 Siemeling, U., Rittinghaus, S., Weidner, T., Brison, J., Castner, D., 2010. COOH-terminated
744 SAMs on gold fabricated from an azobenzene derivative with a 1,2-dithiolane
745 headgroup. Applied Surface Science 256, 1832–1836.
746 https://doi.org/10.1016/j.apsusc.2009.10.015
747 Sun, H., 2004. A Universal Molecular Descriptor System for Prediction of LogP, LogS,
748 LogBB, and Absorption. J. Chem. Inf. Comput. Sci. 44, 748–757.
749 https://doi.org/10.1021/ci030304f
750 Sun, H., Yost, G.S., 2008. Metabolic Activation of a Novel 3-Substituted Indole-Containing
751 TNF-α Inhibitor: Dehydrogenation and Inactivation of CYP3A4. Chem. Res. Toxicol.
752 21, 374–385. https://doi.org/10.1021/tx700294g
753 Tretjakov, A., Syritski, V., Reut, J., Boroznjak, R., Öpik, A., 2016. Molecularly imprinted
754 polymer film interfaced with Surface Acoustic Wave technology as a sensing platform
755 for label-free protein detection. Analytica Chimica Acta 902, 182–188.
756 https://doi.org/10.1016/j.aca.2015.11.004

US EPA [WWW Document], n.d. . US EPA. URL https://www.epa.gov/ (accessed 7.10.20).

Verma, P., Maire, P., Novák, P., 2011. Concatenation of electrochemical grafting with chemical or electrochemical modification for preparing electrodes with specific surface functionality. Electrochimica Acta 56, 3555–3561. https://doi.org/10.1016/j.electacta.2010.11.055

Wang, H., Zhang, J., Wu, Y., Huang, H., Jiang, Q., 2018. Chemically functionalized two-dimensional titanium carbide MXene by in situ grafting-intercalating with diazonium ions to enhance supercapacitive performance. Journal of Physics and Chemistry of Solids 115, 172–179. https://doi.org/10.1016/j.jpcs.2017.12.039

Wishart, D.S., Knox, C., Guo, A.C., Shrivastava, S., Hassanali, M., Stothard, P., Chang, Z., Woolsey, J., 2006. DrugBank: a comprehensive resource for in silico drug discovery and exploration. Nucleic Acids Res 34, D668–D672. https://doi.org/10.1093/nar/gkj067

Figures and Captions

New contributions to the drug profile of TNFα inhibitor SPD304: affinity, selectivity and ADMET considerations

Aïda Mascret[a,b], Hadley Mouhsine[b], Ghada Attia[c], Damien Cabrera[a], Mohamed Benchekroun[a], Patrick Gizzi[e], Chouki Zerrouki[c], Najla Fourati[c], Jean-François Zagury[a] , Maité Sylla-Iyarreta Veitia[a*], Marc Port[a*]

Affiliations

[a] *Laboratoire Génomique, Bioinformatique et Chimie Moléculaire (EA 7528), Conservatoire National des Arts et Métiers (Cnam), 2 rue Conté, 75003, HESAM Université, Paris, France.*

[b] *Peptinov, Pépinière Paris Santé Cochin,, Hôpital Cochin, 29 rue du Faubourg Saint Jacques Paris 75014*

[c] *Laboratoire SATIE, UMR CNRS 8029, Conservatoire National des Arts et Métiers (Cnam), 292 rue Saint Martin, 75003, HESAM Université, Paris, France*

[c] *PCBIS, UMS3286 CNRS - Université de Strasbourg, Boulevard Sébastien Brant, 67401 Illkirch Cedex*

*Corresponding author (E-mail address):

maite.sylla@lecnam.net (Pr. M. Sylla-Iyarreta Veitía)

marc.port@lecnam.net (Pr. M. Port)

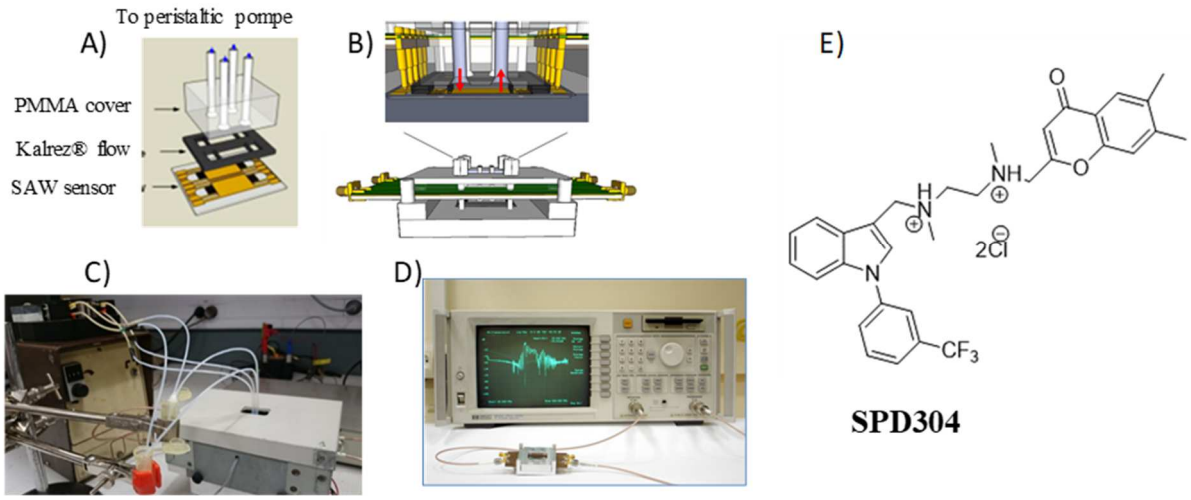

Fig. 1. Schematic representation of a part of the SAW sensor's setup. (A). The various parts of the sensing system. (B). Complete assembly including the printed circuit board. (C). Overview of the system assembly and the fluidic circuit with peristaltic pump. (D). HP8214 network analyser. (E). Structure of SPD304 in dihydrochloride salt form.

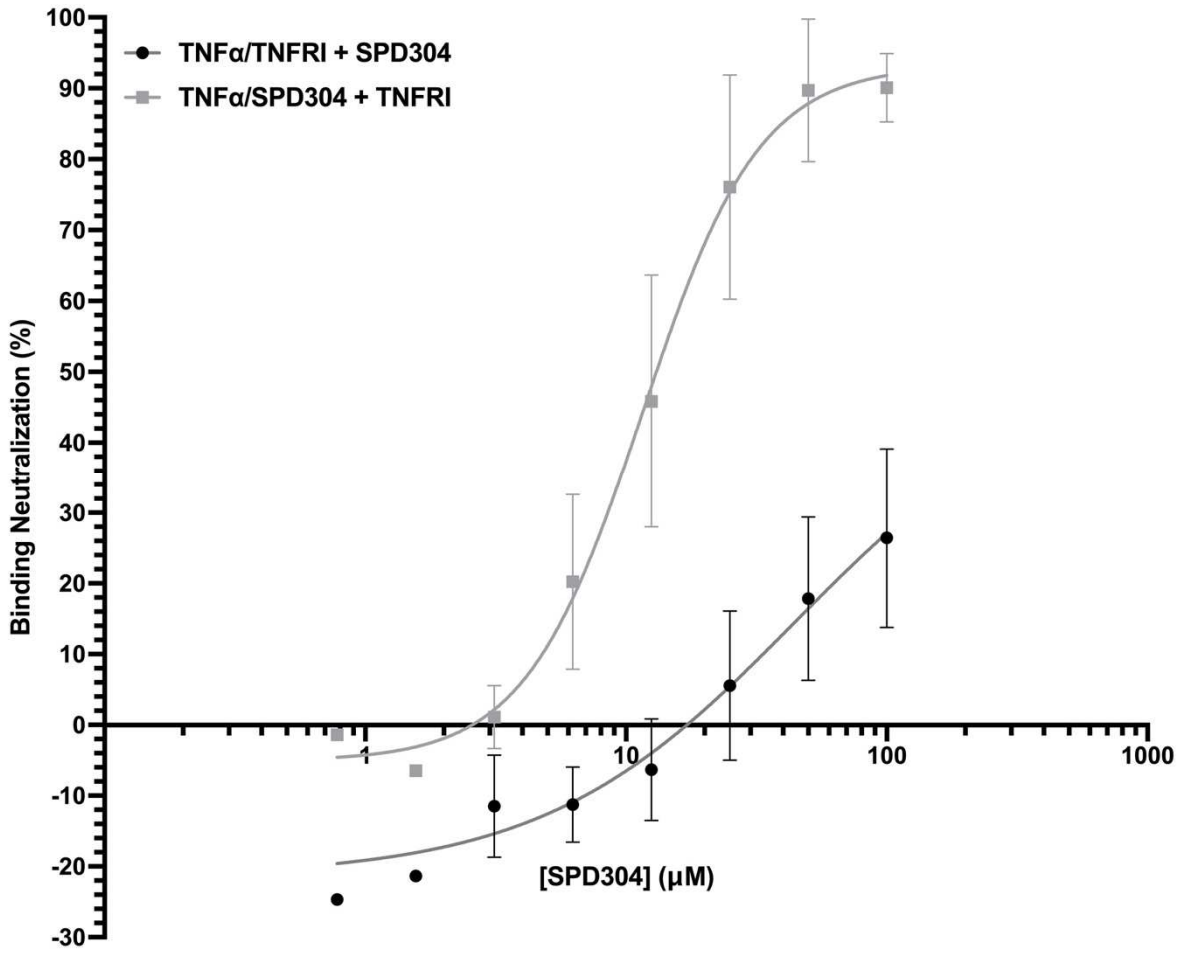

Fig. 2. Effect of SPD304 on the TNFα/TNF receptor 1 equilibrium. SPD304 inhibited TNFα/TNF receptor 1 interaction in a dose-dependent manner. TNFα/SPD304 + TNF receptor 1 IC_{50} = 12 ± 4.5 µM. Data are representative of four experiments.

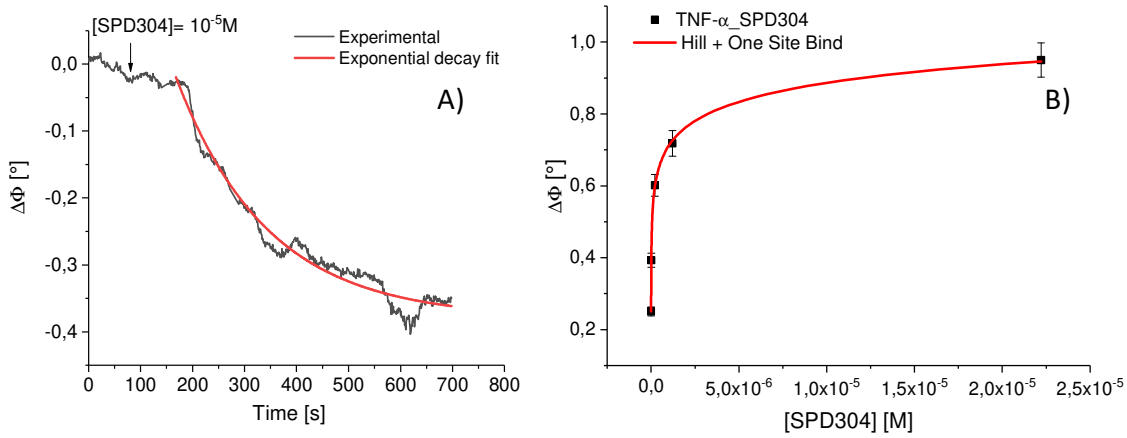

Fig. 3. (A). Phase variations versus time after the injection of 10^{-5} M of SPD304 on the sensing area. (B). Phase-shift variations cumulative ($\Delta\Phi$) versus SPD304 concentration.

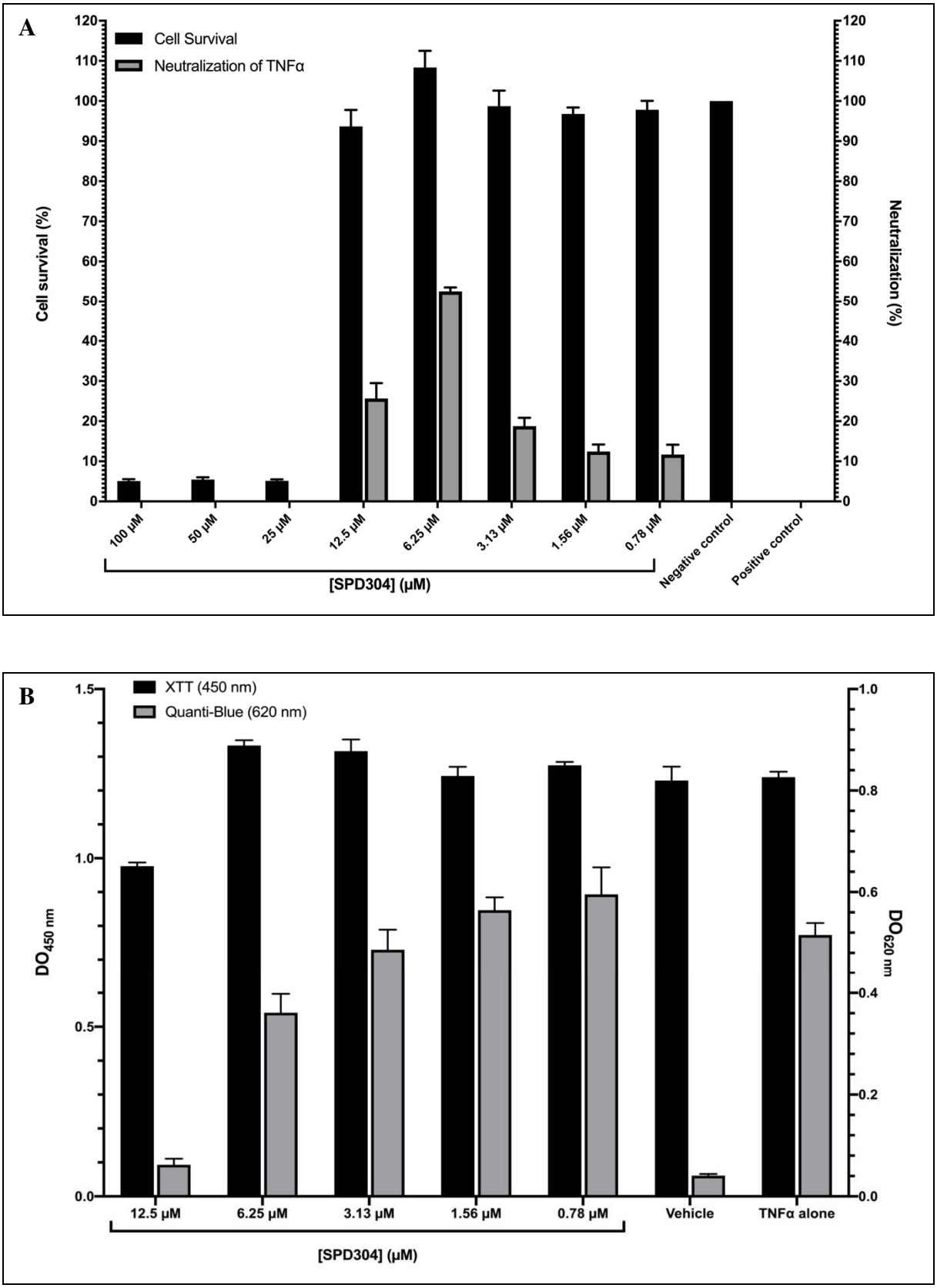

Fig. 4. Effect of SPD304 on L929 and HEK-Blue™ TNFα cell survival and neutralization of TNFα. (**A**). Data represent cell survival of L929 cells in presence of various concentrations of

SPD304 (left axis, black bars) and neutralization of TNFα in presence of TNFα and various concentrations of SPD304 (right axis, grey bars). Due to high toxicity of SPD304, IC_{50} was not calculated but was evaluated at 6.25 µM. (**B**). Data represent cell survival of HEK-Blue™ TNFα cells in presence of various concentrations of SPD304 (XTT, left axis, black bars) and neutralization of TNFα in presence of TNFα and various concentrations of SPD304 (QUANTI-Blue™, right axis, grey bars). Due to high toxicity of SPD304, IC_{50} was not calculated but was evaluated between 12.5 µM and 6.25 µM. Data are representative of three replicates.

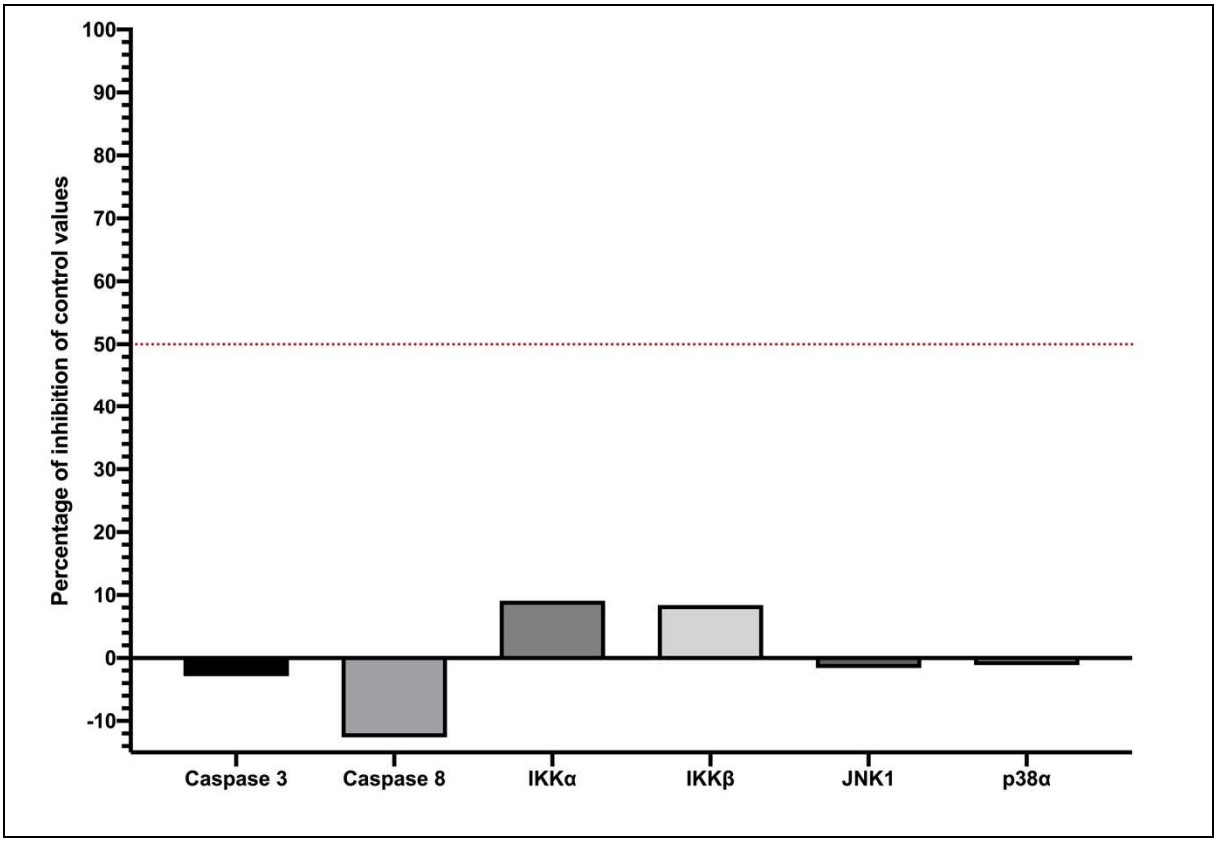

Fig. 5. Effect of direct inhibition of SPD304 on proteins related to TNFα signaling pathway: Caspase 3, Caspase 8, IKKα, IKKβ, JNK1 and p38α. Red line is the cut-off value (50%). Values under this cut-off are considered as negative.

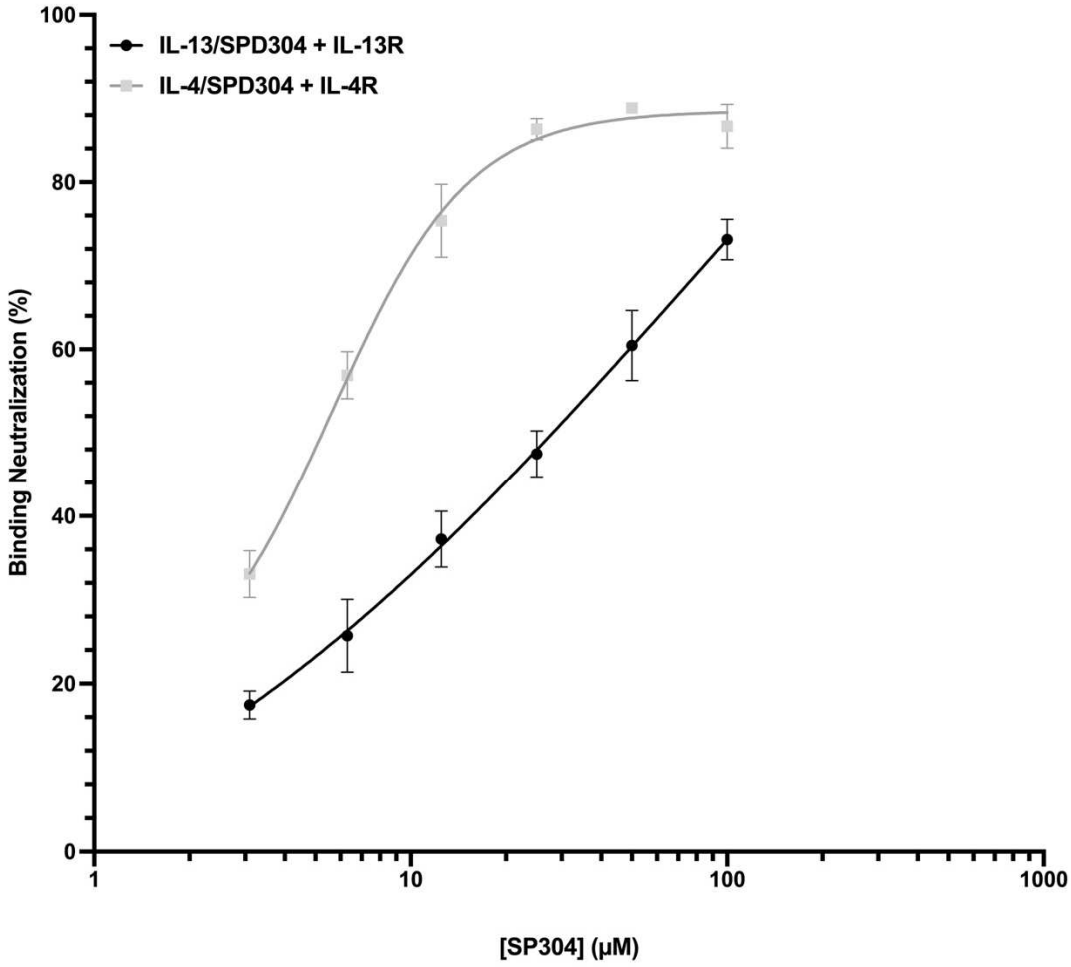

Fig. 6. Effect of SPD304 on the IL-4/IL-4 receptor subunit α and IL-13/IL-13 receptor α2 equilibria. SPD304 inhibited IL-4/IL-4 receptor subunit α and IL-13/IL-13 receptor α2 interaction in a dose-dependent manner. IL-4/IL-4 receptor subunit α IC_{50} = 6 μM, IL-13/IL-13 receptor α2 IC_{50} = 79 μM. Data are representative of three replicates.

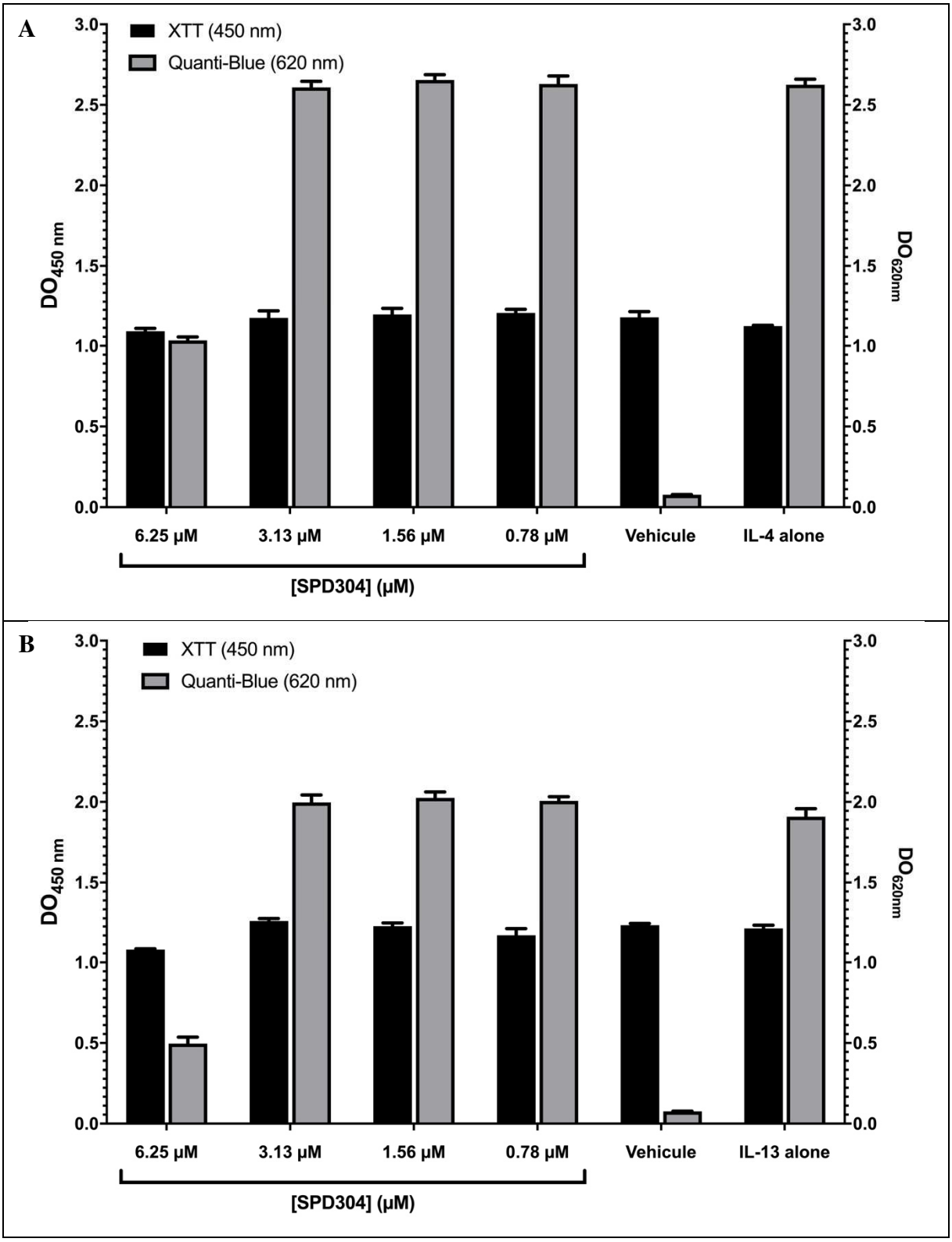

*Fig. 7. Effect of SPD304 on HEK-Blue™ IL-4/IL-13 cell survival and neutralization of IL-4 and IL-13. (**A**). Data represent cell survival of HEK-Blue™ IL-4/IL-13 cells in presence of various concentrations of SPD304 (XTT, left axis, black bars) and neutralization of IL-4 in*

*presence of IL-4 and various concentrations of SPD304 (QUANTI-Blue™, right axis, grey bars). Due to high toxicity of SPD304, IC_{50} was not calculated but was evaluated at between 6.25 et 3.125 µM. (**B**). Data represent cell survival in presence of various concentrations of SPD304 (XTT, left axis, black bars) and neutralization of IL-13 in presence of IL-13 and various concentrations of SPD304 (QUANTI-Blue™, right axis, grey bars). Due to high toxicity of SPD304, IC_{50} was not calculated but was evaluated at between 6.25 et 3.125 µM. Data are representative of three replicates.*

Tables

New contributions to the drug profile of TNFα inhibitor SPD304: affinity, selectivity and ADMET considerations

Aïda Mascret[a,b], Hadley Mouhsine[b], Ghada Attia[c], Damien Cabrera[a], Mohamed Benchekroun[a], Patrick Gizzi[e], Chouki Zerrouki[c], Najla Fourati[c], Jean-François Zagury[a] , Maité Sylla-Iyarreta Veitia[a*], Marc Port[a*]

Affiliations

[a] *Laboratoire Génomique, Bioinformatique et Chimie Moléculaire (EA 7528), Conservatoire National des Arts et Métiers (Cnam), 2 rue Conté, 75003, HESAM Université, Paris, France.*

[b] *Peptinov, Pépinière Paris Santé Cochin,, Hôpital Cochin, 29 rue du Faubourg Saint Jacques Paris 75014*

[c] *Laboratoire SATIE, UMR CNRS 8029, Conservatoire National des Arts et Métiers (Cnam), 292 rue Saint Martin, 75003, HESAM Université, Paris, France*

[c] *PCBIS, UMS3286 CNRS - Université de Strasbourg, Boulevard Sébastien Brant, 67401 Illkirch Cedex*

*Corresponding author (E-mail address):

maite.sylla@lecnam.net (Pr. M. Sylla-Iyarreta Veitía)

marc.port@lecnam.net (Pr. M. Port)

Table 1. ADMET parameters predicted for SPD304.

Physicochemical properties							
	MW[a]	**cLogD[b]**	**cLogP[c]**	**Solubility[d]**	**HBA[e]**	**HBD[f]**	**TPSA[g]**
	547.61	3.1	6.9	0.8	5	0	41.62
Absorption							
	Caco-2 P_{app}[h]	**P-gp inhibition[i]**	**P-gp substrate[j]**	**% HIA[k]**			
Category	Moderately permeable	Inhibitor	Non substrate	Moderately absorbed			
Probability	-	91%	61%	-			
Value	$14x10^{-6}$	-	-	81%			
Pharmacokinetics and distribution							
	F (20%) bioavailability)[l]	**F (30 %) bioavailability)[m]**	**%PBB[n]**	**V_d (L/Kg)[o]**	**Half-life (hour)[p]**	**CL_{int}[q]**	
Category	F20+	F30+	Highly bound	Evenly distributed	-	-	
Probability	68%	53%	94%	-	-	-	
Value	-	-	-	0.42	2.23	1.64	
Metabolism							
Oxydation[r]	**CYP1A2**	**CYP3A4**	**CYP2C9**	**CYP2C19**	**CYP2D6**		
Substrate[s]	Yes	Yes	No	Yes	No		
Substrate probability	58%	74%	49%	70%	48%		
Inhibitor[t]	Yes	Yes	Yes	Yes	Yes		
Inhibitor probability	66%	78%	46%	88%	53%		
Toxicity							
	hERG[u]	**H-HT[v]**	**Mutagenicity[w]**	**DILI[x]**			
Category	Blocker	Positive	Negative	Positive			
Probability	91%	71%	63%	67%			

[a] MW: molecular weight ($g.mol^{-1}$)

[b] cLogD: calculated distribution coefficient at pH 7.4: < 1: solubility high; permeability low by passive transcellular diffusion; permeability possible via paracellular if MW < 200; metabolism low. 1 to 3: solubility moderate; permeability moderate; metabolism low. 3 to 5:

solubility low; permeability high; metabolism moderate to high. > 5: solubility low; permeability high; metabolism high.

[c] cLogP: calculated octanol-water partition coefficient (lipophilicity)

[d] solubility (µg/ml): < 10 µg/ml: low solubility; 10–60 µg/ml: moderate solubility; > 60 µg/ml: high solubility

[e] HBA: hydrogen bond acceptor

[f] HBD: hydrogen bond donor

[g] TPSA: total polar surface area in Å²

[h] Caco-2 permeability: P_{app} < 2 x 10^{-6} cm.s^{-1}: low permeability; 2x10^{-6} < P_{app} < 20x10^{-6} cm.s^{-1}: moderate permeability; P_{app} > 20x10^{-6} cm.s^{-1}: high permeability.

[i] P-gp inhibition: inhibition of P-gp has shown to be responsible for several clinical drug-drug interactions.

[j] P-gp substrate: more likely to be a P-gp substrate: N+O ≥ 8; MW > 400; acid with pKa > 4. More likely to be a P-gp non-substrate: N+O ≤ 4; MW < 400; acid with pKa < 8

[k] %HIA: percentage of human intestinal absorption

[l] F (20% bioavailability): ≥ 20%: F20+; < 20%: F20-

[m] F (30% bioavailability): ≥ 30%: F30+; < 30%: F30-

[n] %PPB: percentage of plasma protein binding

[o] V_d: volume of distribution. < 0.07 l/kg: confined to blood, bound to plasma protein or highly hydrophilic; 0.07-0.7 l/kg: evenly distributed; > 0.7 l/kg: bound to tissue components (e.g., protein, lipid), highly lipophilic.

[p] Half-life ($t_{1/2}$, h): Range: > 8 hours: high; 3 < $t_{1/2}$ < 8 hours: moderate; < 3 hours: low

[q] Clearance CL_{int}: Range: > 15 ml.min^{-1}.kg^{-1}: high; 5 < CL_{int} < 15 ml.min^{-1}.kg^{-1}: moderate; <5 ml.min^{-1}.kg^{-1}: low

[r] Most common chemical reaction of phase 1 metabolism (oxidation) by cytochromes P450 CYPxxx

[s] Substrate: substrate classification models (yes/no) for human CYPxxx

[t] Inhibitor: inhibitor classification models (yes/no) for human CYPxxx

[u] hERG liability: Features may lead to hERG blocker: A basic amine (positively ionizable, pKa > 7.3). Hydrophobic/lipophilic substructure(s) (clogP > 3.7). Absence of negatively ionizable groups or oxygen H-bond acceptors.

[v] H-HT: Human hepatotoxicity

[w] Ames mutagenicity test: Ames positive & negative: significantly induces revertant colony growth at least in one out of usually five strains, otherwise, negative.

[x] DILI: Drug induced liver injury